Progress In Electromagnetics Research C, Vol. 172, 371–378, 2026
PIER C

(Received 23 June 2026, Accepted 24 July 2026, Scheduled 18 August 2026)

A Stable Multi-Band Bandpass Negative Group Delay Circuit with Ultra-Low Insertion Loss

Zhiyang Feng[1], Aixia Yuan[1,*], Junzheng Liu[2], Yuwei Meng[1], and Hongjun Zhang[1]

[1]*School of Information Science and Engineering, Dalian Polytechnic University, Dalian 116034, China*
[2]*Dalian SeaSky Automation Co., Ltd., Dalian, China*

ABSTRACT: Negative group delay (NGD) circuits are important for signal delay compensation in RF and microwave systems. However, realizing multiple NGD passbands with low insertion loss and compact size remains challenging. This paper proposes a compact lumped-element tri-band bandpass NGD circuit for low-frequency RF applications. The proposed circuit consists of three parallel resonant branches. Theoretical modeling, parameter analysis, circuit simulation, and experimental measurements are carried out to investigate the NGD characteristics. The fabricated prototype exhibits NGD responses at 46 MHz, 90 MHz, and 146 MHz. The measured group delays are -3.35 ns, -2.13 ns, and -1.41 ns, respectively, while the corresponding insertion losses are 1.807 dB, 1.638 dB, and 1.495 dB. The fractional NGD bandwidths reach 36.96%, 18.88%, and 12.90%. The proposed lumped-element topology provides compact size, low insertion loss, and tri-band NGD performance, making it suitable for low-frequency RF delay compensation and multi-band signal-processing applications.

1. INTRODUCTION

In radio frequency (RF) and microwave signal-processing systems, the amplitude response of a circuit is not the only factor that determines signal quality. The phase slope, usually described by group delay, also affects waveform integrity, timing accuracy, and pulse transmission. When a signal passes through filters, matching networks, interconnects, or delay-sensitive front-end circuits, a nonuniform group delay may lead to waveform spreading and phase distortion. Therefore, group delay control has become an important issue in the design of wideband and multi-band RF circuits. Negative group delay (NGD) circuits provide an effective method for compensating for positive delays within a limited frequency band. Instead of implying noncausal signal transmission, an NGD response is produced by a controlled phase characteristic in a physically realizable network. Early NGD studies mainly focused on basic synthesis and delay compensation mechanisms [1, 2]. Subsequent studies extended the NGD concept to RC networks, feedback operational amplifier structures, transmission line circuits, and sensor delay-compensation networks [3, 4]. These studies show that NGD circuits can be used as functional phase-compensation units in practical electronic and microwave systems. Among the different NGD responses, bandpass NGD circuits are particularly useful because they provide delay compensation only around the required operating band. More recent studies have further investigated complementary split-ring resonator (CSRR)- and defected ground structure (DGS)-based NGD circuits, broadband NGD circuits with enhanced flatness, and multi-band NGD circuits with low insertion loss [5–8]. These structures improve the achievable NGD bandwidth, insertion loss, and operating frequency flexibility. However, many reported designs rely on transmission-line or coupled-line sections. Such implementations are suitable for microwave frequencies but may occupy a relatively large area when the target operating frequency is reduced to the MHz range. In addition, realizing multiple NGD passbands in one compact structure remains challenging, especially when low insertion loss and flexible frequency allocation are required simultaneously. Therefore, multi-band NGD circuits have attracted increasing attention. Dual-band and tri-band NGD circuits have been developed for multi-band wireless systems [9, 10]. More recent studies have further investigated CSRR-DGS-based NGD circuits, broadband NGD circuits with enhanced flatness, and multi-band NGD circuits with low insertion loss [5–8]. These studies confirm the feasibility of multi-band NGD behavior; however, there is still room to simplify the circuit configuration and improve its suitability for low-frequency RF applications. In this study, a compact lumped-element tri-band bandpass NGD circuit is proposed. The circuit consists of three parallel resonant branches, and each branch contributes to one NGD passband through its frequency-dependent admittance and phase responses. Although the proposed tri-band topology is constructed by connecting three single-band NGD branches in parallel, its design is not a simple superposition of three independent cells. The off-resonant admittance of each branch contributes to the total shunt admittance and may shift the center frequencies, weaken the NGD values, or increase the insertion loss of the other bands. Therefore, the component values of the three branches are coordinately selected to obtain three distinguishable NGD passbands while limiting the additional loading introduced by the non-target branches. This coordinated parameter design enables the circuit to achieve tri-

* Corresponding author: Aixia Yuan (yuanax@dlpu.edu.cn).

band NGD operation with relatively balanced group-delay responses and low insertion loss. Compared with distributed microstrip implementations, the proposed lumped-element topology is more convenient for low-frequency RF designs and compact integration. The main contributions of this study are as follows. First, a compact tri-band bandpass NGD circuit is realized through the coordinated design of three parallel lumped resonant branches, taking into account loading effects among branches. Second, the relationship between the lumped-element values and NGD characteristics was analyzed through theoretical modeling and parametric simulation. Third, a prototype circuit was fabricated and measured to verify the proposed design. The measured results demonstrate three NGD passbands with low insertion loss, showing the potential of the proposed topology for RF delay compensation and multi-band signal-processing applications.

Compared with previously reported multi-band NGD circuits in [9, 10, 17], the main advantage of the proposed design lies in its suitability for low-frequency RF implementation. Distributed NGD circuits generally require transmission-line or resonator sections whose physical dimensions increase considerably as the operating frequency decreases. In contrast, the proposed circuit is implemented using lumped resistors, inductors, and capacitors, and its physical size is therefore not directly determined by the operating wavelength. In addition, the three NGD operating frequencies can be adjusted through component-level parameter selection without redesigning the physical dimensions of transmission-line sections. These characteristics make the proposed topology more convenient for compact MHz-range NGD circuits and low-frequency delay-compensation applications.

2. CIRCUIT STRUCTURE AND THEORETICAL ANALYSIS

2.1. Single-Band NGD Cell

The proposed single-band bandpass NGD cell is implemented using a lumped resonant branch, as illustrated in Fig. 1. The branch consists of a series RLC path and a parallel RL path. For the single branch, the equivalent impedance is expressed as

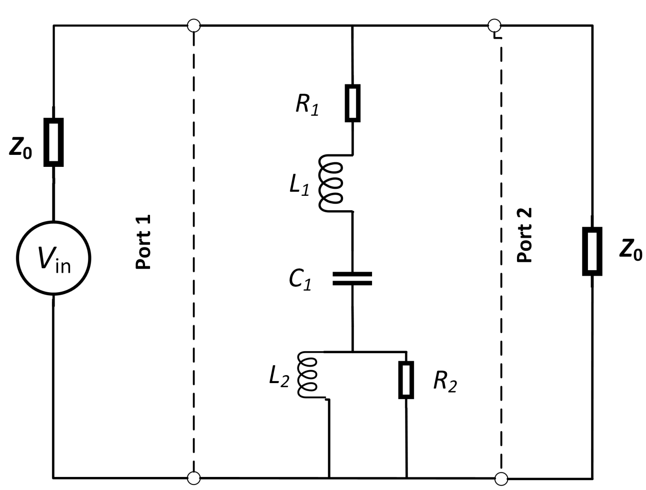

FIGURE 1. Topology of the proposed single-band bandpass NGD cell.

Equation (1):

$$Z_1(j\omega) = \frac{\left(R_1 + j\omega L_1 + \dfrac{1}{j\omega C_1}\right)(R_2 + j\omega L_2)}{R_1 + R_2 + j\omega(L_1 + L_2) + \dfrac{1}{j\omega C_1}}. \quad (1)$$

Here, R_1, L_1, and C_1 denote the resistance, inductance, and capacitance in the series RLC path, respectively, while R_2 and L_2 denote the resistance and inductance in the parallel RL path, respectively. For the single-band cell, only one resonant branch is used, and the corresponding input admittance is expressed as Equation (2):

$$Y_{\text{in}}(j\omega) = \frac{1}{Z_1(j\omega)}. \quad (2)$$

The proposed topology was selected because the series RLC path and parallel RL path provide complementary tuning functions. The series inductance and capacitance mainly determine the operating frequency, whereas the resistive elements and the parallel inductance provide additional control of the phase slope, NGD magnitude, bandwidth, and insertion loss. Compared with a conventional single-resonant RLC branch, this composite structure offers more degrees of freedom for balancing the NGD response and transmission loss. It is also suitable for multi-band extension because several branches with different resonant frequencies can be directly connected in parallel.

2.2. Tri-Band NGD Circuit

To obtain three NGD passbands, three resonant branches with different lumped element values are connected in parallel, as shown in Fig. 2. Therefore, the total admittance of the circuit is written as Equation (3):

$$Y_{\text{total}}(j\omega) = \sum_{i=1}^{3} \frac{1}{Z_i(j\omega)}. \quad (3)$$

The impedances of the three branches are given by Equation (4):

$$\begin{cases} Z_1(j\omega) = \dfrac{\left(R_1 + j\omega L_1 + \dfrac{1}{j\omega C_1}\right)(R_4 + j\omega L_4)}{R_1 + R_4 + j\omega(L_1 + L_4) + \dfrac{1}{j\omega C_1}}, \\ Z_2(j\omega) = \dfrac{\left(R_2 + j\omega L_2 + \dfrac{1}{j\omega C_2}\right)(R_5 + j\omega L_5)}{R_2 + R_5 + j\omega(L_2 + L_5) + \dfrac{1}{j\omega C_2}}, \\ Z_3(j\omega) = \dfrac{\left(R_3 + j\omega L_3 + \dfrac{1}{j\omega C_3}\right)(R_6 + j\omega L_6)}{R_3 + R_6 + j\omega(L_3 + L_6) + \dfrac{1}{j\omega C_3}}. \end{cases} \quad (4)$$

For the tri-band circuit, R_i, L_i, and C_i ($i = 1, 2, 3$) represent the series RLC parameters of the three branches.

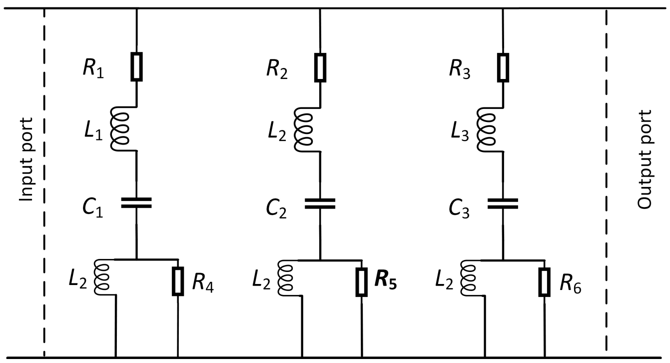

FIGURE 2. Topology of the proposed tri-band bandpass NGD circuit.

Compared with a single-band cell, a tri-band circuit provides multiple frequency-dependent admittance paths. Each resonant branch introduces a local phase variation around its operating frequency, and the superposition of the three branch admittances produces three NGD passbands in a compact lumped-element network.

2.3. Transmission Coefficient

Because the proposed branches are connected as a shunt admittance network, the $ABCD$ matrix can be expressed as Equation (5):

$$\begin{bmatrix} A & B \\ C & D \end{bmatrix} = \begin{bmatrix} 1 & 0 \\ Y_{\text{total}}(j\omega) & 1 \end{bmatrix}. \tag{5}$$

For a two-port network with a characteristic impedance Z_0, the transmission coefficient is calculated as Equation (6):

$$S_{21}(j\omega) = \frac{2}{A + \dfrac{B}{Z_0} + CZ_0 + D}. \tag{6}$$

Substituting Equation (5) into Equation (6), the transmission coefficient becomes Equation (7):

$$S_{21}(j\omega) = \frac{2}{2 + Z_0 Y_{\text{total}}(j\omega)}. \tag{7}$$

For the single-band case, Equation (7) can be reduced to Equation (8):

$$S_{21}(j\omega) = \frac{2}{2 + \dfrac{Z_0}{Z_1(j\omega)}}. \tag{8}$$

The input reflection coefficient of the proposed shunt-admittance network can also be derived from its $ABCD$ matrix as:

$$S_{11}(j\omega) = \frac{A + B/Z_0 - CZ_0 - D}{A + B/Z_0 + CZ_0 + D}. \tag{9}$$

Substituting the $ABCD$ parameters in Equation (5) gives:

$$S_{11}(j\omega) = -\frac{Z_0 Y_{\text{total}}(j\omega)}{2 + Z_0 Y_{\text{total}}(j\omega)}. \tag{10}$$

This expression is used to evaluate reflection characteristics of the proposed tri-band NGD circuit.

2.4. Group Delay, Insertion Loss, and NGD Bandwidth

The phase of the transmission coefficient is defined as Equation (11):

$$\phi(\omega) = \arg\left[S_{21}(j\omega)\right]. \tag{11}$$

The group delay is calculated by Equation (12):

$$\tau_g(\omega) = -\frac{d\phi(\omega)}{d\omega}. \tag{12}$$

For the i-th NGD band, the center angular frequency is defined as the frequency at which the group delay reaches its minimum value within the corresponding negative-group-delay interval:

$$\omega_{0i} = \arg\min_{\omega \in \Omega_i} \tau_g(\omega), \tag{13}$$

It should be noted that the direct criterion for NGD occurrence is:

$$\tau_g(\omega) < 0. \tag{14}$$

The derivative $d\tau_g/d\omega$ only describes the variation of the group-delay response with frequency and does not independently determine whether the group delay is negative. Therefore, the NGD frequency interval in this work is defined by the two zero-crossing frequencies satisfying $\tau_g(\omega) = 0$. Ω_i denotes the frequency interval satisfying $\tau_g(\omega) < 0$. Therefore, the center frequency satisfies:

$$\left.\frac{d\tau_g(\omega)}{d\omega}\right|_{\omega=\omega_{0i}} = 0, \qquad \left.\frac{d^2\tau_g(\omega)}{d\omega^2}\right|_{\omega=\omega_{0i}} > 0. \tag{15}$$

Because the proposed branch contains a composite series-parallel resonant network, substituting the branch impedance into the transmission coefficient leads to a high-order nonlinear equation involving R_{si}, L_{si}, C_{si}, R_{pi}, L_{pi}, and Z_0. Consequently, a compact explicit expression for the exact NGD center frequency is not physically transparent. For initial component selection, the center frequency can be approximately estimated from the dominant series LC resonance as:

$$f_{0i,\text{est}} \approx \frac{1}{2\pi\sqrt{L_{si}C_{si}}}. \tag{16}$$

The final NGD center frequency is then obtained by numerically solving the stationary condition of the complete group-delay expression. The difference between the estimated and exact center frequencies results from the parallel RL path and the loading effects of the other branches.

The circuit exhibits NGD behavior when:

$$\tau_g(\omega) < 0. \tag{17}$$

For the i-th branch, the lower and upper angular-frequency boundaries, ω_{i1} and ω_{i2}, are the two solutions of:

$$\tau_g\left(\omega; \mathbf{p}_i\right) = 0, \tag{18}$$

where

$$\mathbf{p}_i = [R_{si}, L_{si}, C_{si}, R_{pi}, L_{pi}] \tag{19}$$

denotes the branch-parameter vector. Therefore, the NGD bandwidth can be expressed as:

$$BW_i = \frac{\omega_{i2}(\mathbf{p}_i) - \omega_{i1}(\mathbf{p}_i)}{2\pi}. \tag{20}$$

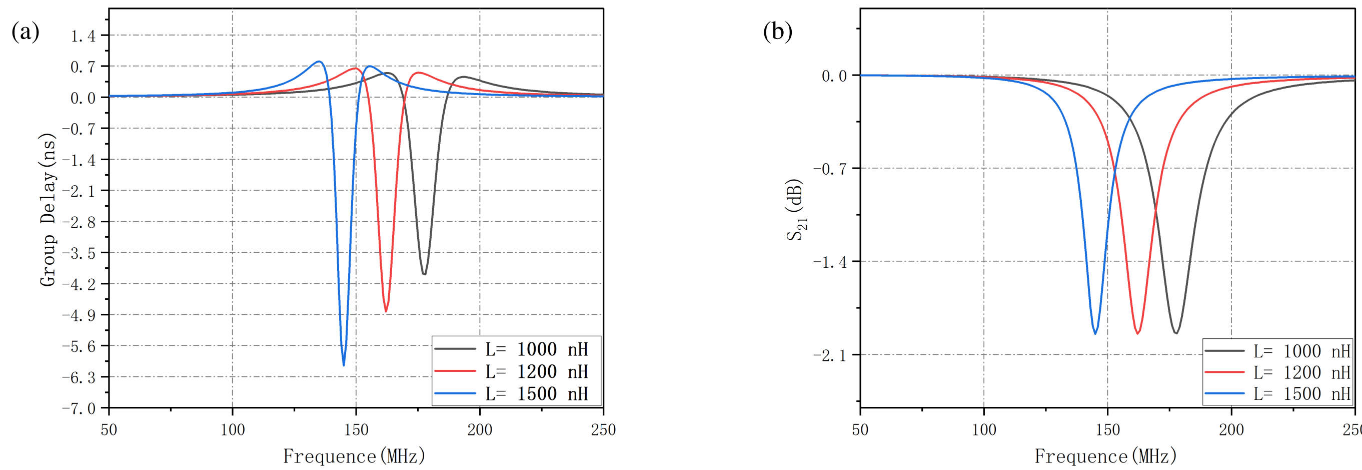

FIGURE 3. Simulation results with different L_1 values. (a) Group delay and (b) S_{21}.

Because the complete group-delay expression contains both series and parallel resonant terms, an explicit bandwidth expression would result in a high-order nonlinear equation and provide limited physical insight. In practical design, L_{si} and C_{si} are mainly used to allocate the operating frequency, whereas R_{si}, R_{pi}, and L_{pi} are adjusted to balance the NGD magnitude, bandwidth, and insertion loss.

The insertion loss is obtained from the magnitude of S_{21}:

$$IL = -20\log_{10}|S_{21}(j\omega)|. \tag{21}$$

The lower and upper boundaries of the NGD band are extracted from the two zero-crossing frequencies of the group-delay curve. When $\tau_g(\omega_1) = 0$ and $\tau_g(\omega_2) = 0$, the corresponding frequency boundaries are as follows:

$$f_1 = \frac{\omega_1}{2\pi}, \qquad f_2 = \frac{\omega_2}{2\pi}. \tag{22}$$

The NGD bandwidth and fractional NGD bandwidth are then defined as:

$$BW = f_2 - f_1, \tag{23}$$

and

$$FBW = \frac{BW}{f_0} \times 100\%, \qquad f_0 = \frac{f_1 + f_2}{2}. \tag{24}$$

3. PARAMETER ANALYSIS OF THE BANDPASS NGD CIRCUIT

3.1. Single-Band NGD Circuit

To evaluate the tuning behavior of the proposed bandpass NGD cell, several parametric simulations were performed by changing one component at a time. During each simulation, the remaining lumped elements were fixed to identify the effect of the selected parameter. The center frequency, group delay, and insertion loss were extracted as the main performance indicators.

It should be noted that the parameter sweeps in the following subsections were performed independently around different reference operating points. Therefore, the fixed component values are not necessarily identical between different sweeps. The statement that the remaining parameters were kept unchanged refers only to each individual parameter sweep.

3.1.1. Effect of L_1

The influence of L_1 was first investigated. The initial values are set as $R_1 = 50\,\Omega$, $L_2 = 1200\,\text{nH}$, $C_1 = 0.8\,\text{pF}$, and $R_2 = 50\,\Omega$. The value of L_1 was changed from 1000 nH to 1500 nH. The extracted results are listed in Table 1, and the simulated group delay and transmission responses are shown in Fig. 3. When L_1 increases from 1000 nH to 1500 nH, the NGD center frequency changes from 41 to 178 MHz. Meanwhile, the group delay varied from -6.036 to -3.994 ns. The insertion loss remained in a narrow range from 1.934 dB to 1.955 dB. These results indicate that L_1 mainly affects the frequency location and phase-slope response of the NGD band, whereas its effect on the transmission magnitude is limited. Because the proposed cell is a composite series-parallel resonant branch, the extracted NGD center frequency is determined by the overall phase variation rather than by a simple LC resonance alone.

TABLE 1. Performance of the bandpass NGD circuit with different L_1 values.

L_1 (nH)	NGD at f_0 (ns)	IL (dB)	f_0 (MHz)
1000	-6.036	1.955	41
1200	-4.770	1.934	103
1500	-3.994	1.938	178

3.1.2. Effect of C_1

The effect of capacitance C_1 was investigated using a separate reference parameter set, while all other elements were fixed during this sweep. The fixed parameters were $L_1 = 1200\,\text{nH}$, $R_1 = 50\,\Omega$, $R_2 = 50\,\Omega$, and $L_2 = 560\,\text{nH}$. Three capacitance values, namely 0.8 pF, 2 pF, and 10 pF, are considered. The results are summarized in Table 2, and the simulated responses

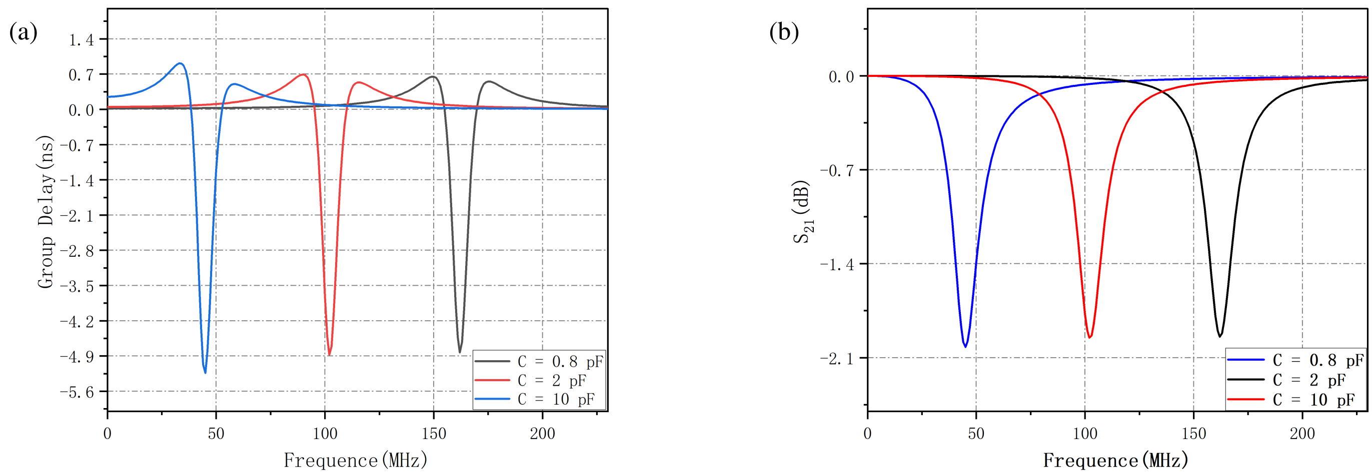

FIGURE 4. Simulation results with different C_1 values. (a) Group delay and (b) S_{21}.

TABLE 2. Performance of the bandpass NGD circuit with different C_1 values.

C_1 (pF)	NGD at f_0 (ns)	IL (dB)	f_0 (MHz)
0.8	-5.237	2.020	45
2	-4.876	1.952	102
10	-4.832	1.944	162

are shown in Fig. 4. As C_1 changes from 0.8 pF to 10 pF, the extracted center frequency moves from 45 to 162 MHz. The corresponding group delay changes slightly from -5.237 to -4.832 ns, and the insertion loss remains close to 2 dB. This shows that C_1 effectively adjusts the NGD operating frequency, whereas the loss level is relatively insensitive to capacitance variation in the simulated range. The results also suggest that the NGD response is governed by the combined impedance of the series RLC and parallel RL paths.

3.2. Tri-Band NGD Circuit

Based on the single-band cell, a tri-band NGD circuit was constructed using three resonant branches. In this section, L_1, L_2, and L_3 are assigned the same value in each simulation case, whereas $C_1 = 0.8$ pF, $C_2 = 2$ pF, $C_3 = 10$ pF, $L_4 = L_5 = L_6 = 560$ nH, and $R_1 = R_2 = R_3 = R_4 = R_5 = R_6 = 50\,\Omega$ are kept fixed. The simulated results are presented in Table 3, and the corresponding curves are shown in Fig. 5. When the inductance is increased from 1000 nH to 1500 nH, all three NGD bands shift simultaneously. For example, the three center frequencies changed from 49, 122, and 178 MHz to 40, 91, and 145 MHz, respectively. The group-delay values also become larger in magnitude, changing from -4.22, -3.09, and -3.89 ns to -6.60, -5.86, and -5.93 ns, respectively. By contrast, the insertion loss remains approximately 2 dB for all three bands. Therefore, inductors L_1, L_2, and L_3 provide an effective way to tune the frequency distribution and NGD level of the tri-band circuit without causing obvious additional loss.

The interactions among the three branches are inherently included in the total-admittance model and full-circuit simulation.

TABLE 3. Performance of the tri-band NGD circuit with different L_1, L_2, and L_3 values.

L_1, L_2, L_3	f_0 (MHz)	NGD at f_0 (ns)	IL (dB)
1000 nH	49	-4.22	2.02
	122	-3.09	2.01
	178	-3.89	2.00
1200 nH	45	-5.13	2.00
	102	-4.71	2.03
	162	-4.71	1.99
1500 nH	40	-6.60	1.99
	91	-5.86	2.04
	145	-5.93	1.98

A systematic investigation of independent branch tuning and coupling effects will be considered in future work.

3.3. Experimental Verification

A prototype of the tri-band NGD circuit was fabricated to validate the proposed design. The component values of the fabricated tri-band NGD circuit are listed in Table 4. The fabricated circuit was implemented on a two-layer FR-4 substrate with a finished thickness of 1.6 mm. The nominal circuit-board dimensions are 30 mm$\times$25 mm, as shown in Fig. 6. The spe-

TABLE 4. Component values of the fabricated tri-band NGD circuit.

Component parameters	Value
L_1, L_2, L_3	1200 nH
L_4	560 nH
L_5	1000 nH
L_6	1500 nH
C_1	0.8 pF
C_2	2 pF
C_3	10 pF
R_1, R_2, R_3, R_4, R_5, R_6	50 Ω

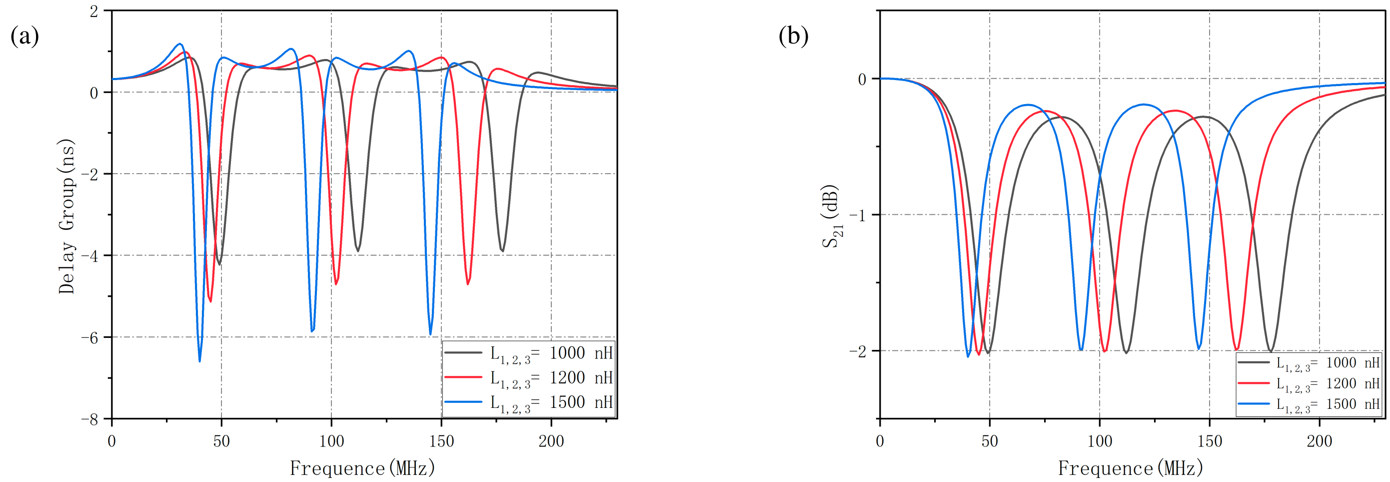

FIGURE 5. Simulation results with different L_1, L_2, and L_3 values. (a) Group delay and (b) S_{21}.

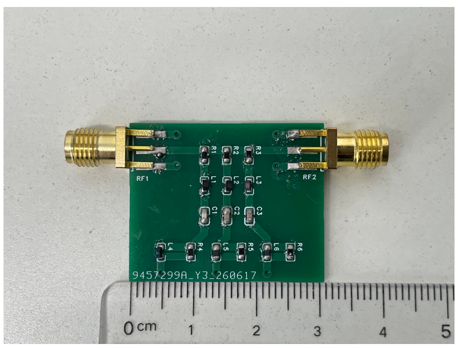

FIGURE 6. Photograph of the fabricated tri-band NGD circuit.

cific laminate grade, dielectric constant, and loss tangent were not provided by the printed circuit board (PCB) manufacturer. Since the proposed circuit is implemented using lumped components without distributed transmission-line resonators, the substrate parameters are not involved in the analytical circuit model. The fabricated circuit was measured using an AV3656A vector network analyzer with a frequency range of 100 kHz–3 GHz. Before measurement, a previously generated full two-port calibration file was loaded into the vector network analyzer to compensate for the systematic errors of the instrument and test cables. No additional de-embedding of the SMA connectors or PCB feeding lines was performed. Therefore, their residual losses and phase effects were included in the measured results. The theoretical, simulated, and measured responses are compared in Fig. 7. It should be emphasized that the theoretical and simulated curves in Fig. 7 were calculated using the component values listed in Table 4, which are identical to the nominal values used in the fabricated prototype. The parameters of the 1500-nH case in Table 3 were used only for the parametric analysis in Section 3.2 and were not used to generate Fig. 7. The measured results show three clear NGD responses at 46 MHz, 90 MHz, and 146 MHz. At these frequencies, the measured group delays are −3.35 ns, −2.13 ns, and −1.41 ns, respectively. The corresponding insertion losses are 1.807 dB, 1.638 dB, and 1.495 dB, while the fractional NGD bandwidths are 36.96%, 18.88%, and 12.90%. The theoretical, simulated, and measured reflection coefficients are further compared in Fig. 8. The measured curves follow the simulated trends, confirming that the proposed topology can realize tri-band bandpass NGD characteristics. Small differences among the calculated, simulated, and measured results can be attributed to the parasitic effects of lumped components, fabrication tolerances, soldering uncertainty, and measurement non-idealities. The main sources of measurement uncertainty include the residual calibration error, connector repeatability, component tolerances, soldering parasitics, and the finite quality factors of the practical lumped components. Even with these practical factors, the prototype maintains distinct NGD responses in three frequency bands. The comparison in Table 5 further shows that the proposed design achieves low insertion loss and competitive NGD bandwidth compared with previously reported bandpass NGD circuits.

As shown in Table 5, the circuit in [9] employs a distributed microstrip topology and operates above 1 GHz. Although it realizes three NGD bands, its physical dimensions are inherently related to the operating wavelength, and its measured insertion losses exceed 16 dB. Therefore, this design is less suitable for compact low-frequency RF applications.

The lumped-element circuits in [18–21] provide more relevant comparisons because they operate in the MHz or sub-GHz frequency range. In particular, the passive RLC-parallel circuit in [21] achieves an NGD response at 227.1 MHz, which is closer to the operating range of the proposed circuit than the previously reported GHz-range distributed designs. However, it realizes only one NGD band and exhibits a measured insertion loss of 8.84 dB.

By comparison, the proposed circuit simultaneously achieves three NGD bands at 46, 90, and 146 MHz, with measured insertion losses of only 1.807, 1.638, and 1.495 dB, respectively. In addition, the fabricated prototype occupies an area of 30 mm×25 mm. These results demonstrate the advantages of the proposed design in terms of simultaneous multi-band operation, low insertion loss, and compact low-frequency implementation.

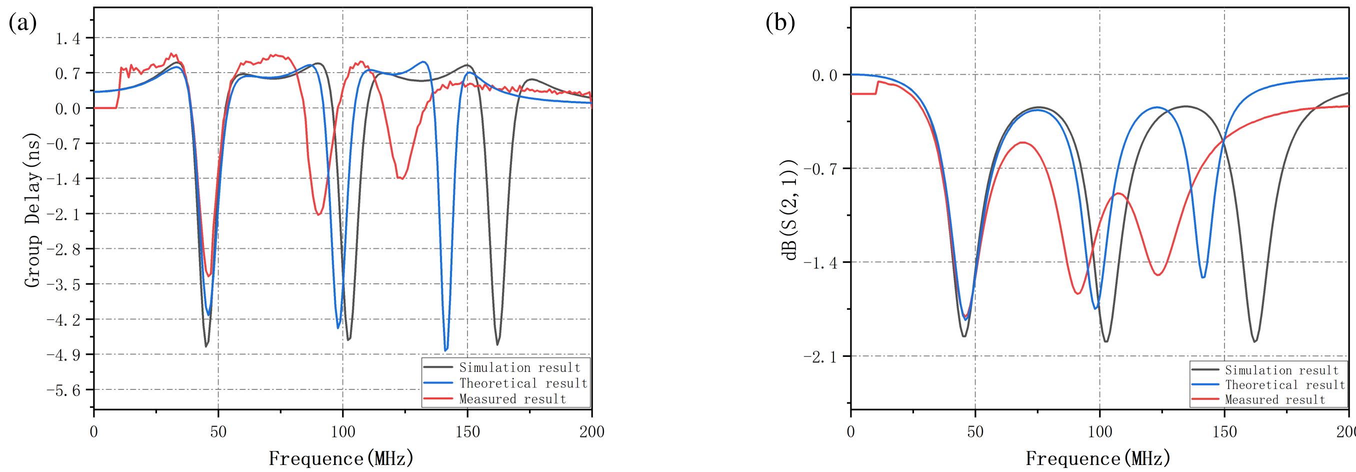

FIGURE 7. Comparison among the theoretical, simulated, and measured results of the tri-band NGD circuit. The theoretical and simulated results were obtained using the same component values as those listed in Table 4 and used in the fabricated prototype. (a) Group delay and (b) S_{21}.

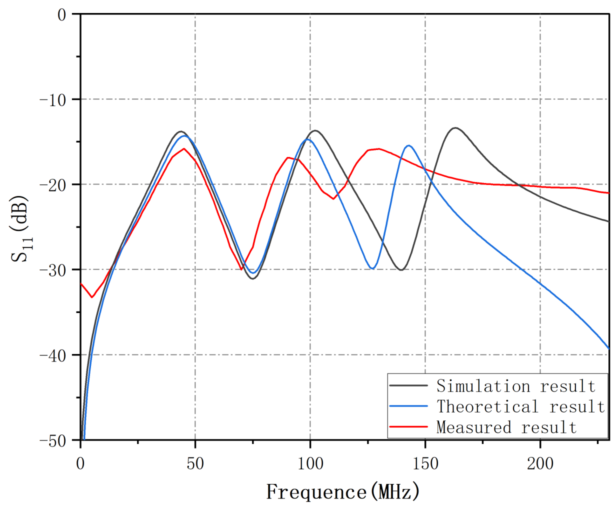

FIGURE 8. Comparison among the theoretical, simulated, and measured S_{11} responses of the proposed tri-band NGD circuit.

TABLE 5. Performance comparison between the proposed tri-band NGD circuit and previously reported bandpass NGD circuits.

Reference	Implementation and topology	Circuit size	f_0 (MHz)	IL (dB)	NGD at f_0 (ns)	NGD FBW
[9]	Distributed microstrip tri-band circuit	20 mm×34.5 mm	1200	16.4	−1.08	12.40%
			3500	24.6	−1.19	8.60%
			5800	18.9	−1.09	3.59%
[15]	Inductorless integrated NGD circuit	N.R.	480	23.0	−0.20	–
			180	27.0	−1.00	–
[16]	Lumped-element multi-band NGD circuit	41 mm×28 mm	70	3.29	−3.99	38.33%
			170	3.31	−3.47	13.70%
			220	3.18	−3.12	10.41%
[17]	Lumped-element multi-band bandpass NGD circuit	N.R.	130	5.81	−2.17	–
			180	5.83	−2.05	–
			240	5.87	−1.90	–
[18]	Lumped-element RLC-parallel BP-NGD circuit	N.R.	227.1	8.84	−8.115	19.46%
This work	Lumped-element tri-band bandpass NGD circuit	30 mm×25 mm	46	1.807	−3.35	36.96%
			90	1.638	−2.13	18.88%
			146	1.495	−1.41	12.90%

N.R. indicates that the physical circuit dimensions were not explicitly reported in the corresponding reference.

4. CONCLUSION

A compact lumped-element tri-band bandpass NGD circuit was proposed and experimentally demonstrated. The circuit uses three parallel resonant branches to produce three independent negative group delay (NGD) passbands. Theoretical analysis shows that the transmission coefficient can be derived from the total shunt admittance of the resonant branch. Parametric simulations further indicate that lumped inductors and capacitors can adjust the frequency allocation and group-delay level of the NGD bands. The fabricated prototype achieved measured NGD responses at 46 MHz, 90 MHz, and 146 MHz. The corresponding group delays are -3.35, -2.13, and -1.41 ns, and the insertion losses are 1.807, 1.638, and 1.495 dB, respectively. The measured fractional NGD bandwidths were 36.96%, 18.88%, and 12.90%. These results verify that the proposed lumped-element topology can provide a tri-band NGD behavior with a low transmission loss. Compared with existing bandpass NGD circuits, the proposed design offers a compact structure and is suitable for low-frequency RF applications. Future work will consider parasitic parameters of practical components during the design stage and introduce optimization algorithms to further improve the device's NGD bandwidth, insertion loss, and frequency controllability.

ACKNOWLEDGEMENT

The authors would like to thank their colleagues and laboratory members for their helpful discussions and technical support during this study. The authors declare that no funding was received for this study.

REFERENCES

[1] Lucyszyn, S., I. D. Robertson, and A. H. Aghvami, "Negative group delay synthesiser," *Electronics Letters*, Vol. 29, No. 9, 798–800, 1993.

[2] Broomfield, C. D. and J. K. A. Everard, "Broadband negative group delay networks for compensation of microwave oscillators and filters," *Electronics Letters*, Vol. 36, No. 23, 1931–1933, 2000.

[3] Wan, F., T. Gu, B. Ravelo, B. Li, J. Cheng, Q. Yuan, and J. Ge, "Negative group delay theory of a four-port rc-network feedback operational amplifier," *IEEE Access*, Vol. 7, 75 708–75 720, 2019.

[4] Wan, F., X. Miao, B. Ravelo, Q. Yuan, J. Cheng, Q. Ji, and J. Ge, "Design of multi-scale negative group delay circuit for sensors signal time-delay cancellation," *IEEE Sensors Journal*, Vol. 19, No. 19, 8951–8962, 2019.

[5] Meng, Y., Z. Wang, S. Fang, T. Shao, H. Liu, and Z. Chen, "Dual-band negative group delay microwave circuit with low signal attenuation and arbitrary frequency ratio," *IEEE Access*, Vol. 8, 49 908–49 919, 2020.

[6] Zhou, X., T. Gu, L. Wu, F. Wan, B. Li, N. M. Murad, S. Lalléchère, and B. Ravelo, "S-matrix and bandpass negative group delay innovative theory of Ti-geometrical shape microstrip structure," *IEEE Access*, Vol. 8, 160 363–160 373, 2020.

[7] Ravelo, B., F. Wan, J. Nebhen, W. Rahajandraibe, and S. Lalléchère, "Resonance effect reduction with bandpass negative group delay fully passive function," *IEEE Transactions on Circuits and Systems II: Express Briefs*, Vol. 68, No. 7, 2364–2368, 2021.

[8] Vauché, R., R. A. B. Mefteh, F. Haddad, J. Nebhen, W. Rahajandraibe, F. Wan, S. LALLéchère, and B. Ravelo, "Experimental time-domain study for bandpass negative group delay analysis with lill-shape microstrip circuit," *IEEE Access*, Vol. 9, 24 155–24 167, 2021.

[9] Meng, Y., Z. Wang, S.-J. Fang, and H. Liu, "A tri-band negative group delay circuit for multiband wireless applications," *Progress In Electromagnetics Research C*, Vol. 108, 159–169, 2021.

[10] Yuan, A., S. Fang, Z. Wang, and H. Liu, "A novel multifunctional negative group delay circuit for realizing band-pass, high-pass and low-pass," *Electronics*, Vol. 10, No. 14, 1742, 2021.

[11] Ji, Q., T. Gu, Z. Gao, M. Yang, Y. Yuan, H. Du, F. Wan, N. M. Murad, G. Fontgalland, H. S. Silva, and B. Ravelo, "Csrr dgs-based bandpass negative group delay circuit design," *IEEE Access*, Vol. 11, 20 309–20 318, 2023.

[12] Meng, Y., P. Li, A. Yuan, and Z. Lan, "Compact broadband negative group delay circuit with flatness and bandwidth enhancement," *Electronics*, Vol. 13, No. 15, 3056, 2024.

[13] Nako, J., C. Psychalinos, A. S. Elwakil, and B. J. Maundy, "A note on the bandwidth of negative group delay filters," *International Journal of Circuit Theory and Applications*, Vol. 53, No. 1, 477–484, 2025.

[14] Gurgel, N. B., G. Fontgalland, I. S. Q. Jr., S. M. Holanda, B. Agnus, J. Rossignol, and B. Ravelo, "Compact quadband NGD microstrip circuit for 2–6 GHz ISM bands," *Progress In Electromagnetics Research M*, Vol. 134, 1–12, 2025.

[15] Chen, Z., Y. Song, T. Zhang, B. Yan, and C. Fan, "Design of a novel ultra-low-frequency inductorless negative group delay chip," in *2024 International Conference on Microwave and Millimeter Wave Technology (ICMMT)*, 1–3, Bejing, China, 2024.

[16] Yuan, A., X. Guo, Y. Meng, J. Liu, and N. Chang, "Design of multi-band circuit with negative group delay and lower insertion loss characteristics," *AEU — International Journal of Electronics and Communications*, Vol. 189, 155596, 2025.

[17] Chang, N., A. Yuan, Y. Wang, and J. Liu, "Multi-band pass negative group delay circuit with low insertion loss," *International Journal of Circuit Theory and Applications*, Vol. 53, No. 3, 1292–1301, 2025.

[18] Sambatra, E. J. R., Y. C. M. Boussougou, L. Ramifidisoa, J.-P. Kouadio, S. Ngoho, A. Jaomiary, and N. M. Murad, "Band Pass Negative Group Delay demonstration on a VHF RLC parallel passive lumped circuit," *Advanced Electromagnetics*, Vol. 11, No. 1, 9–21, 2022.